




Driven dust-charge fluctuation and chaotic ion dynamics in the plasma sheath and presheath regions

Mridusmita Das , Suniti Changmai, and Madhurjya P. Bora 

Department of Physics, Gauhati University, Guwahati 781014, India

 (Received 4 January 2023; accepted 15 September 2023; published 5 October 2023)

Possible existence of chaotic oscillations in ion dynamics in the sheath and presheath regions of a dusty plasma, induced by externally driven dust-charge fluctuation, is presented in this work. In a complex plasma, dust charge fluctuation occurs continuously with time due to the variation of electron and ion currents flowing into the dust particles. In most of the works related to dust-charge fluctuation, theoretically it is assumed that the average dust-charge fluctuation follows the plasma perturbation, while in reality, the dust-charge fluctuation is a semirandom phenomenon, fluctuating about some average value. The very cause of dust-charge fluctuation in a dusty plasma also points to the fact that these fluctuations can be driven externally by changing electron and ion currents to the dust particles. With the help of a *hybrid*-particle in cell-Monte Carlo collision (*h*-PIC-MCC) code in this work, we use the plasma sheath as a candidate for driving the dust-charge fluctuation by periodically exposing the sheath-side wall to UV radiation, causing photoemission of electrons, which in turn drive the dust-charge fluctuation. We show that this *driven* dust-charge fluctuation can induce a chaotic response in the ion dynamics in the sheath and the presheath regions.

DOI: [10.1103/PhysRevE.108.045202](https://doi.org/10.1103/PhysRevE.108.045202)

I. INTRODUCTION

Even after decades of active and fruitful research, complex plasmas and plasma sheath continue to enjoy immense attention in present-day plasma physics research. In this work, we bring together the important domains of complex plasmas (also known as dusty plasma), plasma sheath, and the rich tapestry of nonlinear dynamics. While dusty plasma deals with the physics of plasmas with relatively massive and charged dust particles, electrons, ions, and neutrals, it can very well be studied in the context of a plasma sheath, as the presence of charged dust particles significantly modifies the sheath properties and can unravel complex plasma behavior in the sheath and presheath regions [1–7]. Through a *hybrid*-particle in cell-Monte Carlo collision (*h*-PIC-MCC) code, in this work we use the plasma sheath as a candidate to *drive* the dust-charge fluctuation, which in turn induces a chaotic response in the ion dynamics in the vicinity of the sheath. The *h*-PIC-MCC code in question has been developed by two of the authors of this paper, which can handle dusty plasma dynamics with various boundary conditions and has already been benchmarked for different electron and ion dynamics in the electron-plasma, ion-acoustic, and dust-ion-acoustic timescales [8–10]. As a nonlinear plasma environment is essentially multidimensional, the possibility of chaos is invariably there. However, it is quite difficult to directly observe chaotic oscillations in naturally occurring plasmas as well as laboratory plasmas in contrast to carefully controlled plasma environments with some kinds of driving mechanisms. We note that chaotic oscillations are observed in various configurations such as in plasma-diode experiments [11], filamentary discharge plasmas in the presence of plasma bubbles [12], etc. Theoretically, numerous works explore the possibility of

chaos in different plasma environments. Such examples can be found in chaotic Alfvén waves in the context of driven Hamiltonian systems [13], wave-wave interaction [14], quasilinear diffusions [15], etc. Chaotic signals are usually quite common in driven systems, which can be found over a wide range of disparate physical configurations. For example, chaotic signals can be detected in a driven NbSe₃ charge-density wave conductor, as reported by Levy *et al.* [16,17].

So far as the dust-charge fluctuation in a complex plasma is concerned, we realize that in reality, the amount of charge acquired by the dust particles in a plasma is never constant, but fluctuates continuously, owing to the changing electron and ion currents to the dust particles. While the semirandom nature of dust-charge fluctuation in time is quite natural and occurs due to the nonlinear nature of the plasma, theoretically it has been customary to assume these fluctuations to be closely following the plasma perturbation present in the system [5,6,9,10,18]. As the amount of charge on a dust particle varies according to the electron and ion currents to the dust particle, one can also externally *drive* the fluctuation by varying these currents. One such situation is to expose the dust particles to intermittent (or periodic) bursts of charged particles which can cause the dust-charge to fluctuate. Due to the nonlinearity present in the system, there is a possibility that this driven dust-charge fluctuation can induce a chaotic response in the dynamics of the system. Though such a situation in the dust-acoustic regime has been considered by Momeni *et al.* [19], where they have shown a chaotic regime to exist in the oscillation of the dust density, the subject has been largely unexplored. The case of driven dust-charge fluctuation can also be compared to the effect of charged debris moving in a plasma, usually relevant in space plasmas, which has been a subject of some recent studies [20,21].

A. Significance of the work

At this point, it is worthwhile to review the physical conditions, especially in our model, which lead to a chaotic response. As mentioned in the Sec. I, we note that like all multidimensional systems, a plasma system is also prone to chaotic oscillations when the number of dependent variables increases, resulting in distinct dynamical equations. Technically, any multidimensional system having dimensions three or more can exhibit chaos [22]. There are usually three routes [22] via which a periodic oscillation can become a chaotic one: (1) period-doubling, which usually follows a Hopf bifurcation, (2) intermittency, and (3) quasiperiodicity (Ruelle-Takens-Newhouse route) [23]. Out of these three, the intermittency route is usually associated with forced vibration and noise [24]. Right from the time when Lorenz first discovered chaos in 1963, we now know that many natural dynamical systems exhibit chaos [22]. However, a very systematic demonstration of chaotic oscillations is possible often in a controlled environment, where parameters can be adjusted. In this work, we show that by creating periodic bursts of high-energy electrons through photoemission from a sheath-side wall, we can indeed induce a chaotic response in the ion dynamics which is localized to the sheath and the presheath regions. In this work, our purpose is to demonstrate the existence of chaos in a plasma environment which is well realizable in laboratory. Although there are various examples of chaos in plasmas [25], the way we try to induce these oscillations in a plasma system to the best of our knowledge has not been done before, neither theoretically nor experimentally. Beside the fact that our numerical experiment can be easily translated into a real experiment as the parameters and timescales that we use in this work are standard for many low-temperature laboratory plasmas, this work also opens up a regime of nonlinearity in the dust-ion-acoustic domain.

In the context of our driven-dust-charge-fluctuation model, we would particularly like to refer to an earlier experimental work by Nezhlin [26], where chaotic oscillations were shown to have existed in an argon discharge plasma, which appears due to the noise in an external ion source. Subsequently, it has been argued that chaotic oscillations are the result of the interplay between the intrinsic stochasticity of the system and periodically forced oscillation (through the ion beam) [24]. Apparently we shall see that this is what we observe in this work. In Sec. IV we show the stochastic nature of the ion velocity, which turns chaotic in the presence of forced oscillations induced through the plasma sheath.

In Sec. II we develop a dusty plasma model for the plasma sheath, where we describe the sheath structure and develop the sheath equations. In Sec. III we consider the case for driven dust-charge fluctuation and develop our chaotic ion-dynamics model induced by the driven fluctuations. In Sec. IV we describe the *h*-PIC-MCC simulation of the driven dust-charge fluctuation and present the required results. Finally, in Sec. V we conclude.

II. A DUSTY PLASMA MODEL FOR PLASMA SHEATH

Our plasma model consists of electrons, ions, and negatively charged dust particles. The characteristic timescale

of interest is dust-ion-acoustic, where the dust particles are involved in the plasma dynamics *only* through Poisson's equation and the dust-charge fluctuation equation, due to their massive inertia. This is particularly true in our case, as the dust density remains constant which is a reasonable approximation in the dust-ion-acoustic time scale [27,28]. The relevant equations (in one dimension) are ion continuity and momentum equations, with Boltzmann electrons (owing to their negligible mass)

$$\frac{\partial n_i}{\partial t} + \frac{\partial}{\partial x}(n_i u_i) = 0, \quad (1)$$

$$\frac{\partial u_i}{\partial t} + u_i \frac{\partial u_i}{\partial x} = -\frac{1}{m_i n_i} \frac{\partial p_i}{\partial x} - \frac{e}{m_i} \frac{\partial \phi}{\partial x}, \quad (2)$$

$$n_e = n_0 e^{e\phi/T_e}, \quad (3)$$

where the symbols have their usual meanings and the temperature is expressed in energy units. The ion equation of state is used as

$$p_i \propto n_i^\gamma, \quad (4)$$

where γ is the ratio of specific heats. The final equation of the model is Poisson's equation,

$$\epsilon_0 \frac{\partial^2 \phi}{\partial x^2} = e(n_e - n_i + z_d n_d). \quad (5)$$

The dust charge is $q_d = -ez_d$, where we have assumed that the dust particles acquire a net negative charge. Note that the presence of dust grains is incorporated into the model through Poisson's equation only. We use a normalization where the densities are normalized by their respective equilibrium values, $n_j \rightarrow n_j/n_{j0}$, where the subscript "0" refers to the equilibrium values and $j = e, i, d$, respectively, for electrons, ions, and dust particles. The ion velocity u_i is normalized with the ion-sound velocity $c_s = \sqrt{T_e/m_i}$, where $T_{i,e}$ are the ion and electron temperatures, measured in the units of energy and are held constant. The length is normalized with the electron Debye length, and time is normalized by the inverse of ion-plasma frequency (ion-plasma period). The potential ϕ is normalized with (T_e/e) . The dust-charge number z_d is normalized with its equilibrium value $z_{d0} = z_d|_{\phi=0}$. The normalized equations are now

$$\frac{\partial n_i}{\partial t} + \frac{\partial}{\partial x}(n_i u_i) = 0, \quad (6)$$

$$\frac{\partial u_i}{\partial t} + u_i \frac{\partial u_i}{\partial x} + \gamma \sigma n_i^{\gamma-2} \frac{\partial n_i}{\partial x} = -\frac{\partial \phi}{\partial x}, \quad (7)$$

$$n_e = e^\phi, \quad (8)$$

$$\frac{\partial^2 \phi}{\partial x^2} = n_e - \delta_i n_i + \delta_d z_d, \quad (9)$$

where $\delta_i = n_{i0}/n_{e0}$ and $\delta_d = n_d z_{d0}/n_{e0}$ are the ratios of equilibrium densities of ions and dust particles to that of electrons. The quasineutrality condition is given as $\delta_i = 1 + \delta_d$. Note that the dust density remains constant, while the dust-charge fluctuates.

The dust charge q_d for spherical dust particles can be expressed in terms of the dust potential ϕ_d ,

$$q_d = C \Delta V = 4\pi \epsilon_0 r_d \phi_d, \quad (10)$$

where C is the grain capacitance and $\varphi_d = \phi_g - \phi$, ϕ_g being the grain potential. We define the equilibrium dust-charge number z_{d0} in terms of the magnitude of the equilibrium dust potential $\varphi_{d0} = |\varphi_d|_{\phi=0}$,

$$z_{d0} = 4\pi\epsilon_0 r_d e^{-1} \varphi_{d0}, \quad (11)$$

where e is the magnitude of electronic charge and r_d is the radius of a dust particle. By using the relation $q_d = -ez_d$, we can normalize the expression for dust potential

$$z_d = -\alpha\varphi_d, \quad (12)$$

with

$$\alpha = \frac{4\pi\epsilon_0 r_d T_e}{e^2 z_{d0}} \sim N_D, \quad (13)$$

which approximately represents the total number of dust particles N_D , inside a dust Debye sphere. We now consider the dust-charging equation

$$\frac{dq_d}{dt} = I_e + I_i, \quad (14)$$

where $I_{e,i}$ are the electron and ion currents to the dust particles, which can be written as (dimensional) [6]

$$I_i = 4\pi r_d^2 e n_i \left(\frac{T_i}{2\pi m_i} \right)^{1/2} \left(1 - \frac{e\varphi_d}{T_i} \right), \quad (15)$$

$$I_e = -4\pi r_d^2 e n_e \left(\frac{T_e}{2\pi m_e} \right)^{1/2} \exp\left(\frac{e\varphi_d}{T_e} \right). \quad (16)$$

Assuming Boltzmann electron density $n_e = e^\phi$, the normalized dust-charging equation (14) can be written as

$$\begin{aligned} \frac{d\varphi_d}{dt} &= I_{e0} \left[\delta_i \delta_m \sigma^{1/2} n_i \left(1 - \frac{\varphi_d}{\sigma} \right) - \exp(\phi + \varphi_d) \right] \\ &\equiv f(n_i, \phi, \varphi_d), \end{aligned} \quad (17)$$

where

$$I_{e0} = \frac{r_d e^2 n_{e0}}{\epsilon_0 T_e \omega_{pi}} \left(\frac{T_e}{2\pi m_e} \right)^{1/2} \quad (18)$$

is the normalized equilibrium electron current to the dust particles, $\delta_m = \sqrt{m_e/m_i} \approx 0.023$, and $\sigma = T_i/T_e$. Time evolution of average dust-charge \bar{z}_d as obtained from the *hybrid*-PIC-MCC simulation (see Sec. IV for a brief description of the *h*-PIC-MCC model) is shown in Fig. 1 [9]. In the code, both electrons and ions are considered as thermal particles, distributed with their respective distributions. The simulation parameters correspond to a typical laboratory situation with plasma density $n_0 \sim 10^{16} \text{ m}^{-3}$, electron and ion temperatures to be, respectively, $T_e \sim 1 \text{ eV}$ and $T_i \sim 0.01 \text{ eV}$, and an e - i mass ratio of $(m_e/m_i)^{-1} \sim 1835.16$. This corresponds to the electron Debye length of the plasma as $\lambda_{De} \sim 7.4 \times 10^{-5} \text{ m}$. A typical run can have a simulation box length of 0.001–0.1 m, and each species is represented with 10^5 – 10^7 macroparticles [8–10] having particle weighting. The simulation is carried out with equally spaced 1D cells with a cell number of 600–1000. For example, in a simulation box length of 0.004 m, with 10^5 macroparticles for both electrons and ions, equally spaced 600 cells, and the evolution time step of $\sim 10^{-11} \text{ s}$, we can have full spatial resolution with a temporal resolution of the order of the electron timescale.

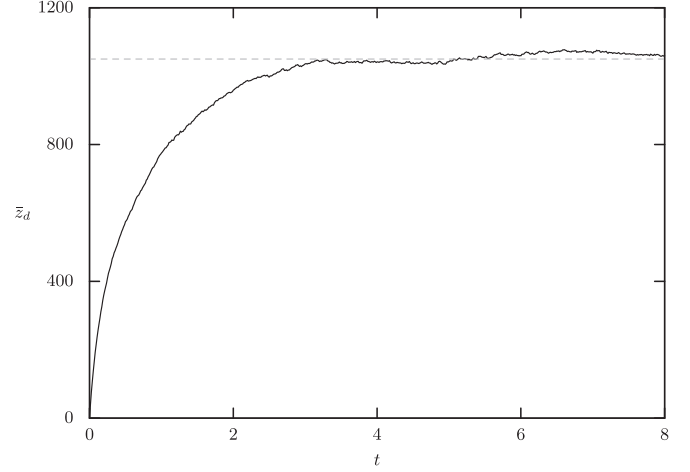


FIG. 1. Charging of dust particles in a dusty plasma. The time is measured in units of the ion-plasma period (inverse of ion-plasma frequency).

A. Sheath equations and sheath structure

Consider now a plasma sheath in a steady state. Far away from the sheath, the plasma potential vanishes and other plasma parameters approach their bulk (equilibrium) values: $x \rightarrow \infty$, $\phi \rightarrow 0$, $u_i \rightarrow u_0 \equiv M$, $p_i \rightarrow 1$, $n_i \rightarrow 1$, $z_d = z_d/z_{d0} \rightarrow 1$. M is the Mach number, which is the ratio of the ion velocity far from the sheath to that of ion-sound velocity. For a stationary sheath, the steady-state equations are

$$\frac{\partial}{\partial x}(n_i u_i) = 0, \quad (19)$$

$$u_i \frac{\partial u_i}{\partial x} + \gamma \sigma n_i^{\gamma-2} \frac{\partial n_i}{\partial x} = -\frac{\partial \phi}{\partial x}, \quad (20)$$

$$u_i \frac{\partial \varphi_d}{\partial x} = f(n_i, \phi, \varphi_d). \quad (21)$$

From the continuity equation, we have

$$n_i = M/u_i. \quad (22)$$

Integration of Eq. (20) thus results in the conservation of total energy flux, which is a combination of the kinetic flux, enthalpy flux, and electrostatic flux,

$$\phi = \frac{1}{2n_i^2} M^2 (n_i^2 - 1) + \frac{\gamma \sigma}{(\gamma - 1)} (1 - n_i^{\gamma-1}). \quad (23)$$

An expression for n_i as a function of ϕ can be found from Eqs. (20) and (22), $n_i = \mathcal{F}(\phi)$. For arbitrary γ , the above equation has to be solved numerically. For $\gamma = 3$, however, we can find an analytical expression for $n_i(\phi)$ as

$$\begin{aligned} n_i &= \frac{1}{2\sqrt{3}\sigma} \left\{ [(M + \sqrt{3}\sigma)^2 - 2\phi]^{1/2} \right. \\ &\quad \left. - [(M - \sqrt{3}\sigma)^2 - 2\phi]^{1/2} \right\}. \end{aligned} \quad (24)$$

The signs in front of the square roots are fixed through the boundary condition on n_i (see the Appendix for an analysis on how different values of γ might affect the results). As the ion density can be expressed as a function of the plasma potential,

$n_i \equiv n_i(\phi)$, Poisson's equation can be integrated to get

$$\frac{1}{2} \left(\frac{d\phi}{dx} \right)^2 + V(\phi, \varphi_d, M, \sigma, \gamma) = 0, \quad (25)$$

where $V(\phi, \varphi_d, M, \sigma, \gamma)$ is the equivalent Sagdeev potential or pseudopotential for a sheath, given by

$$V(\phi, \varphi_d, M, \sigma, \gamma) = 1 - e^\phi + \delta_i \int_0^\phi n_i(\phi) d\phi - \delta_d \int_0^\phi z_d(\phi) d\phi. \quad (26)$$

For real solution, we must have

$$V(\phi, \varphi_d, M, \sigma, \gamma) < 0 \quad (27)$$

for all values of ϕ . We can also determine the minimum velocity for the ions ($u_0 \equiv M$) at the sheath boundary (the Bohm condition) from this condition. The boundary condition on V is, at $\phi = 0$, $V(\phi) = 0$.

A few noteworthy points are in order. If the dust-charge fluctuation is absent, it means the electron and ion currents to the dust particles always balance each other so that at all times we have

$$f(n_i, \phi, \varphi_d) = 0. \quad (28)$$

This equation can be numerically solved for z_d (or for φ_d) as a function of ϕ , and the Sagdeev potential can be constructed numerically. However, in the presence of dust-charge fluctuation, the problem *has* to be solved numerically. Multiplying Eq. (21) with n_i and using Eq. (19), we can write

$$\frac{\partial}{\partial x} (n_i u_i \varphi_d) = n_i f(n_i, \phi, \varphi_d), \quad (29)$$

where we note that $M = n_i u_i$. Thus, using Poisson's equation, Eq. (26), and the above equation, one can summarily construct the following numerical model:

$$\frac{d^2 \phi}{dx^2} = e^\phi - \delta_i n_i - \alpha \delta_d \varphi_d, \quad (30)$$

$$\frac{d\varphi_d}{dx} = \frac{n_i}{M} f, \quad (31)$$

$$n_i = \mathcal{F}(\phi). \quad (32)$$

This problem is a coupled boundary and initial value problem involving a nonlinear Poisson's equation, which needs to be solved with a hybrid approach. We have solved this model with a finite-difference algorithm with a Newton iteration for the nonlinear Poisson's equation with Dirichlet boundary conditions. During every Newton iteration of the boundary value problem, we use a single, fourth-order Runge-Kutta step for the initial value equation, Eq. (31). Of course, in every step, the nonlinear algebraic equation, Eq. (32), needs to be solved for n_i , which we have solved using a nonlinear solver. However, as we shall see, although the boundary values for Poisson's equation can be estimated quite accurately, the same can not be said for the initial value for Eq. (31). This has to be estimated iteratively following the negativity condition (27) for a numerically constructed Sagdeev potential.

The boundary values for the plasma potential can be estimated by considering the current at the wall and infinity. Far from the sheath, the plasma potential *must* approach the bulk

potential, i.e., zero, $\phi|_{x \rightarrow \infty} = 0$. Assuming the current at the wall be zero, for a stationary sheath we have

$$j_e + j_i + j_d = 0, \quad (33)$$

where $j_{e,i,d}$ are the electron, ion, and dust currents to the wall. However, in view of the inertia of the massive dust particles in comparison to the electrons and ions, it can be safely assumed that in the electron and ion timescale, the contribution to the wall current by the dust particles is negligibly small,

$$j_e + j_i \approx 0, \quad (34)$$

for all practical purposes. The electrons, which reach the wall with a minimum velocity v_{\min} by overcoming the negative potential at the wall ϕ_w , contribute to electron current at the wall. So we have

$$v_{\min} = \left(-\frac{2e\phi_w}{m_e} \right)^{1/2}, \quad (35)$$

so that for the electron current, we have

$$j_e = -e \int_{v_{\min}}^{\infty} \int_{-\infty}^{\infty} \int_{-\infty}^{\infty} v f_e(v) dv, \quad (36)$$

where $f_e(v)$ is the electron velocity distribution function. For a Maxwell velocity distribution, we have the expression

$$j_e = -n_{e0} e \left(\frac{T_e}{2\pi m_e} \right)^{1/2} \exp\left(\frac{e\phi_w}{T_e} \right). \quad (37)$$

The ion current at the wall is given by

$$j_i = en_{i0} u_i \left(\frac{T_e}{m_i} \right)^{1/2} = en_0 u_0 \left(\frac{T_e}{m_i} \right)^{1/2}, \quad (38)$$

where u_0 is the ion velocity (the Mach number) at the sheath boundary. From the neutrality condition (34), we can solve for the wall plasma potential (normalized) as

$$\phi_w = -2.84 + \ln M. \quad (39)$$

As the plasma potential vanishes far away from the sheath, we can determine the dust potential as well, from the charging equation as at ∞ , $\partial\varphi_d/\partial x \rightarrow 0$, so that $f(\varphi_d)|_{x \rightarrow \infty} = 0$. This determines the $\varphi_d|_{x \rightarrow \infty} = \varphi_{d\infty}$ as

$$\varphi_{d\infty} = \sigma - W(z), \quad (40)$$

where $W(z)$ is the Lambert W function with

$$z = \frac{\sigma^{1/2}}{\delta_i \delta_m n_i} e^\sigma. \quad (41)$$

Numerically, however, it is *not* possible to use this value as an initial value for solving the dust-charging equation as we need to start at a very large distance from the wall. We realize that although the dust current at the wall is negligible, the dust potential φ_{dw} at the wall need not be so and is expected to be small and negative. So we continue solving the whole model starting with $\varphi_{dw} = 0$ iteratively with the condition that the Sagdeev potential $V(\phi, \varphi_d, M, \sigma, \gamma) < 0$ [29] in the entire sheath region for the defined parameters. The results of this calculation are shown in Fig. 2, where we plot the plasma potential ϕ and the dust potential φ_d as we go away from the sheath to the bulk plasma. The solid lines in each panel indicate the theoretical curves obtained for $\gamma = 5/3$ for

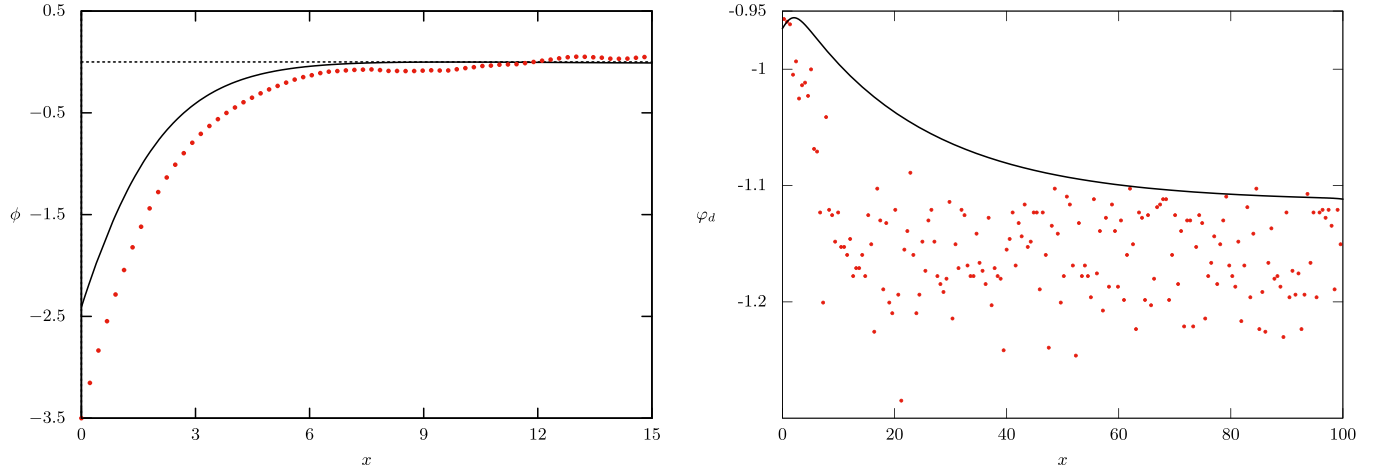


FIG. 2. Normalized plasma potential ϕ and dust potential φ_d with dust-charge fluctuation. The length x is measured in the units of electron Debye length λ_{De} .

$M = 1.5$, and the dots indicate the equivalent results from the h -PIC-MCC simulation with the parameters as mentioned before. We must note that in the simulation, there is no fixed Mach number for the ions as they enter the sheath with different Mach numbers starting with the minimum.

III. DRIVEN DUST-CHARGE FLUCTUATION AND CHAOS

A dynamical model demonstrating chaos in dusty plasma driven by dust-charge fluctuation was formulated by Momeni *et al.* [19,30]. In their work, they reduced the dusty plasma dynamical model to a single, second-order, nonautonomous differential equation in dust density, which exhibits chaotic dynamics in the dust-acoustic regime. This single differential equation is described as a Van der Pol–Mathieu (VdPM) equation owing to its Van der Pol-like term and a Mathieu-like nonautonomous term

$$\frac{d^2 n_d}{dt^2} - (\alpha - \beta n_d^2) \frac{dn_d}{dt} + \omega_0^2 (1 + h \cos \gamma t) n_d = 0, \quad (42)$$

where n_d is the dust density, and $\omega_0 \sim \omega_{pd}$ is the characteristic oscillation frequency of the system of the order of dust-plasma frequency ω_{pd} . The nonautonomous term results from the time-dependent dust-charge fluctuation term, represented by $h \cos \gamma t$, with h as the amplitude of the fluctuation and γ as the fluctuation frequency. As seen from the equation, the dust-charge fluctuation term is supposed to oscillate harmonically. The authors assumed that the dust particles are continuously created and destroyed through a source term αn_d and a loss term $\beta n_d^3/3$ in the 1D dust continuity equation [19]

$$\frac{\partial n_d}{\partial t} + \frac{\partial}{\partial x} (n_d u_d) = \alpha n_d - \frac{1}{3} \beta n_d^3, \quad (43)$$

where the source term is assumed to appear due to the production of charged dust grains through electron absorption and the loss term is due to a three-body recombination term.

It is important to realize that in the above work, though the authors *do not* describe why the time-dependent dust-charge fluctuation term is harmonic, it can be argued to be originating from an externally driven source, such as *photoemission*, which is what we are investigating in this work. In

this work, we provide a prescription where chaotic oscillations are experimentally realizable. Our parameters are, however, in the ion-acoustic (and dust-ion-acoustic) regime, unlike the above model. In what follows, we construct a model which can demonstrate chaotic ion dynamics through *driven* dust-charge fluctuation. There is, however, an important difference between the above-mentioned work and ours, that here we are using the dust-charge fluctuation as a mechanism to drive the chaotic dynamics in ion velocity, whereas, in the former, it is the dust density which shows chaotic behavior.

A. A chaotic ion-dynamics model

We now construct an ion-dynamical model from Eqs. (6)–(9) for the driven dust-charge case, which can exhibit chaos. We introduce a scaled time $\tau = t - x/v_0$ so that the equations can be converted to a single variable, where v_0 is the velocity of the comoving frame from where the observations (numerical) are being made. In terms of the scaled variable, we have $\partial/\partial t \equiv \partial/\partial \tau$ and $\partial/\partial x \equiv -v_0^{-1} \partial/\partial \tau$. So Eqs. (6), (7), and (9) become

$$\frac{\partial n_i}{\partial \tau} - \frac{1}{v_0} \frac{\partial}{\partial \tau} (n_i u_i) = 0, \quad (44)$$

$$\frac{\partial u_i}{\partial \tau} - \frac{u_i}{v_0} \frac{\partial u_i}{\partial \tau} - 2 \frac{\sigma}{v_0} \frac{\partial n_i}{\partial \tau} = \frac{1}{v_0} \frac{\partial \phi}{\partial \tau}, \quad (45)$$

$$\frac{1}{v_0^2} \frac{\partial^2 \phi}{\partial \tau^2} = n_e - \delta_i n_i + \delta_d z_d(\tau), \quad (46)$$

where for simplicity we assumed $\gamma = 2$ (see the Appendix for a justification). Equation (44) can be integrated to obtain the ion density

$$n_i = \frac{v_0 - u_0}{v_0 - u_i}, \quad (47)$$

where we have assumed that at infinity $u_i(\tau) \rightarrow u_0$ and $n_i(\tau) \rightarrow n_{i0} \equiv 1$ (note the normalization). Similarly, Eq. (45) can be integrated to obtain the plasma potential

$$\phi = \frac{1}{2} (u_0^2 - u_i^2) - v_0 (u_0 - u_i) + 2\sigma \left(1 - \frac{v_0 - u_0}{v_0 - u_i} \right), \quad (48)$$

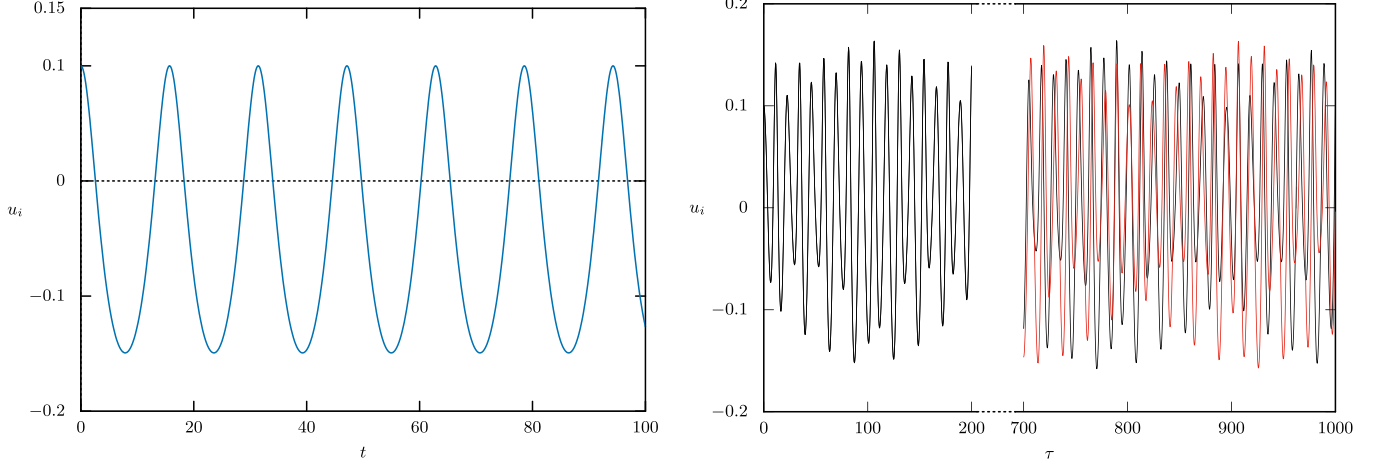


FIG. 3. Periodic oscillations of the system, represented by Eq. (49) in the absence of dust-charge fluctuations (left). On the right, the same oscillations with driven dust-charge fluctuation is presented where the sensitivity to the initial conditions can be clearly seen. All plasma parameters are as in the case of *h*-PIC-MCC simulation. The time t and the scaled time τ are in units of the ion-plasma period, and the velocity is in units of ion-sound speed.

where we have imposed the condition that at infinity (bulk plasma), $\phi(\tau) \rightarrow 0$. Using Poisson's equation and the above expressions, we finally arrive at a coupled 2D nonlinear differential equation in u_i ,

$$\ddot{u}_i A + \dot{u}_i^2 B + C = 0, \quad (49)$$

where the “.” denotes $d/d\tau$ and

$$A = \frac{1}{v_0^2} \left(\mu_i - 2\sigma \frac{\mu_0}{\mu_i^2} \right), \quad (50)$$

$$B = -\frac{1}{v_0^2} \left(1 + 4\sigma \frac{\mu_0}{\mu_i^3} \right), \quad (51)$$

$$C = \delta_i \frac{\mu_0}{\mu_i} - e^\phi - \delta_d z_d(\tau), \quad (52)$$

with $\mu_0 = v_0 - u_0$ and $\mu_i = v_0 - u_i$. With an autonomous term involving the time-varying dust-charge $z_d(\tau)$, Eq. (49) fulfills all the basic characteristics which are necessary for the exhibition of chaotic dynamics. The driven dust-charge term $z_d(\tau)$ can be designed as

$$z_d(\tau) = \varrho \cos(v\tau)^\Delta, \quad (\Delta \in \text{integer}), \quad (53)$$

where ϱ is the amplitude and v is the frequency of the driven dust-charge fluctuation. It can be numerically shown that in the absence of any dust-charge fluctuation, i.e., when $z_d \equiv 1$, for $v_0 > u_0$, Eq. (49) admits periodic solutions (see Fig. 3).

1. Bifurcation analysis

For the purpose of bifurcation analysis, we convert the nonautonomous system represented by Eq. (49) into a system of autonomous equations by introducing two dummy variables $x(t)$ and $y(t)$,

$$\dot{u}_i = v, \quad (54)$$

$$\dot{v}_i = -(v^2 B + C)/A, \quad (55)$$

$$\dot{x} = x(1 - x^2 - y^2) - vy, \quad (56)$$

$$\dot{y} = y(1 - x^2 - y^2) + vx, \quad (57)$$

where $\cos(v\tau)$ in Eq. (53) is replaced by $x(t)$. Note that the last two equations of the above system have stable and unique solutions

$$x(t) = \cos(vt), \quad y(t) = \sin(vt). \quad (58)$$

The above system has two nontrivial equilibrium points $(u_0, 0, 0, 0)$ and $(u_i^*, 0, 0, 0)$ in the (u_i, v_i, x, y) hyperplane, with $u_i^* < 0$. Out of these two, the first one is an equilibrium point of type “center” [22], around which stable periodic orbits exist. The second one is an interesting point around which a saddle-node bifurcation occurs. Though a linear analysis of the above system *does not* indicate a saddle-node, a numerical solution does reveal the existence of a saddle-node bifurcation. This saddle-node bifurcation finally leads to the chaotic behavior. A similar behavior is also seen in a driven nonlinear Alfvén system, where a saddle-node bifurcation ultimately leads to chaotic trajectories [31].

2. $v_0 \gg u_0$

We now explore the regime $v_0 \gg u_0$ in the presence of driven dust-charge fluctuation. Our parameters are $\varrho \sim 0.1$, which is a small positive quantity and $v \sim 0.4$. We take $u_0 \sim 10^{-4}$ and $v_0 \sim 1$. The parameter Δ is set to 2. Note that when $v_0 \gg u_0$, it is as if $\tau \sim t$ and the variables are almost constant in space. This points out to a localized disturbance where chaotic oscillation might be observed. The rest of the plasma parameters are as in the case of the simulation. The results of this analysis are presented in Figs. 3 and 4. The left panel of Fig. 3, shows the periodic oscillations when $z_d = 1$ or equivalently when $\varrho = 0$, i.e., no dust-charge fluctuation. The right panel shows the same oscillations (in black and red) when $\varrho = 0.1$ (the other parameters are as mentioned before). One can clearly see the sensitivity of the oscillations where both

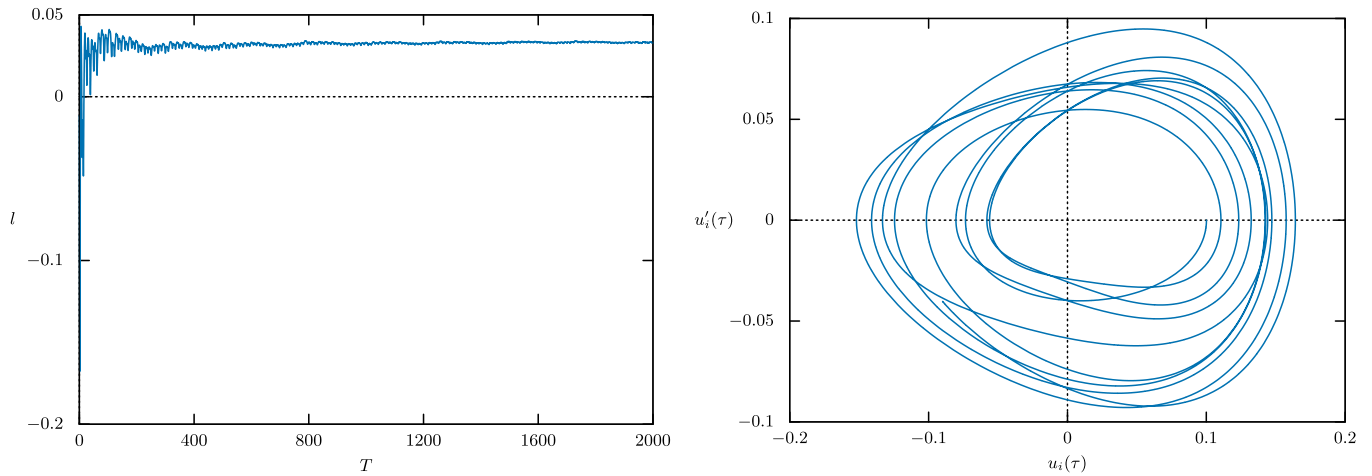


FIG. 4. Maximal Lyapunov exponent l of the system with numerical time step T (left), shown for the first $\tau \sim 500$ and the phase portrait in the chaotic regime (right). The value of $l \sim 0.033$. Velocities are normalized by the ion-sound speed.

of these differ by a factor $\sim 10^{-5}$ in the initial conditions. We carry out a Lyapunov exponent calculation [22] on Eq. (49) for these oscillations, and the results are presented in Fig. 4, where the left panel shows the maximal Lyapunov exponent of the system $l \sim 0.033$, which is positive signifying chaos, and

in the right panel, the phase portrait of the system is shown. In calculating the Lyapunov exponent, we have evolved the system for $\tau \simeq 2000$ with a step size of 0.01, gathering about 2×10^5 points. The corresponding Poincaré plots [22] are shown in Fig. 5, which shows the typical characteristics of

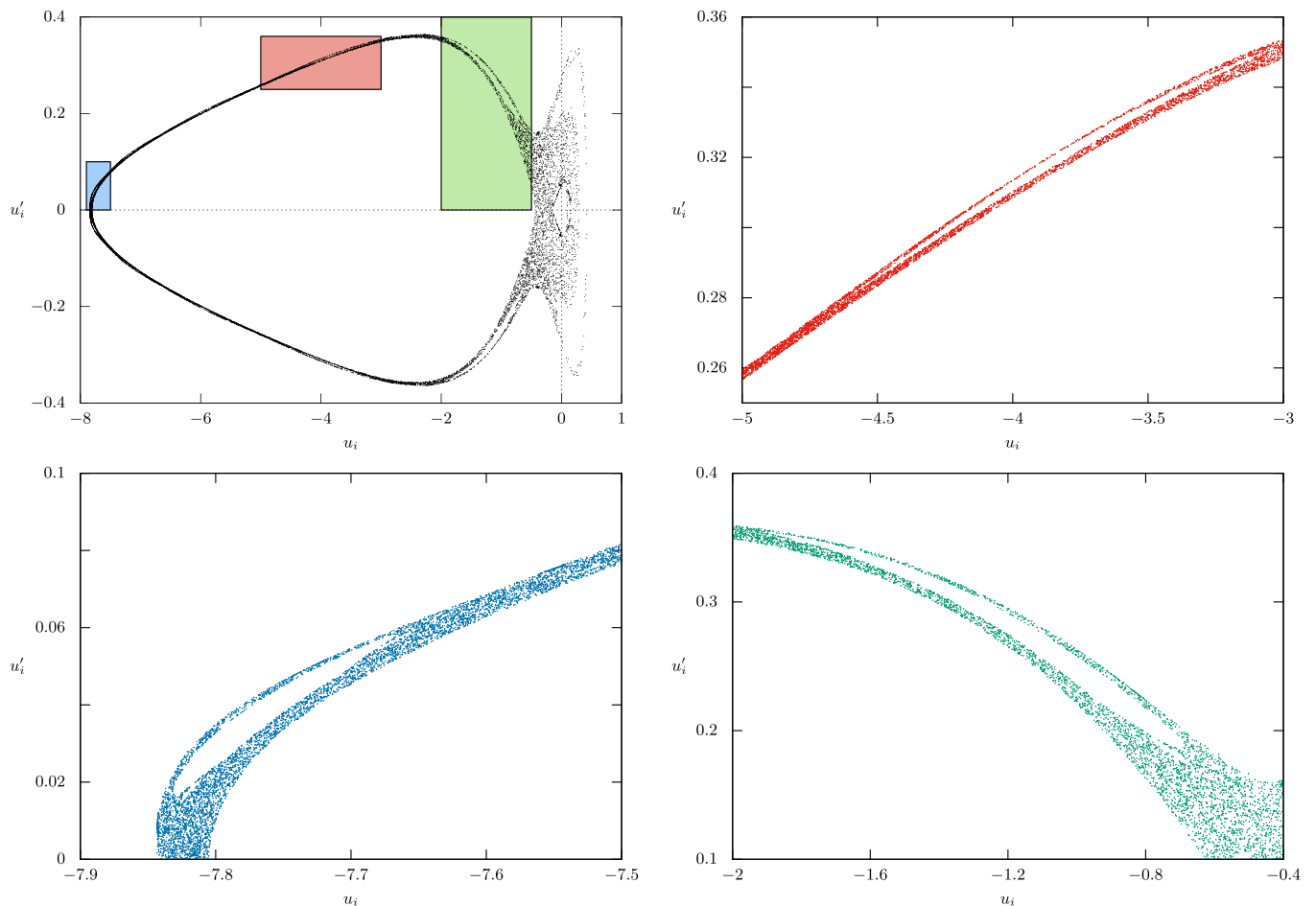


FIG. 5. Poincaré plots for the system in the chaotic regime. Subsequent panels are zoomed-out plots of the corresponding regions shown in the first plot. The velocities are normalized by the ion-sound speed.

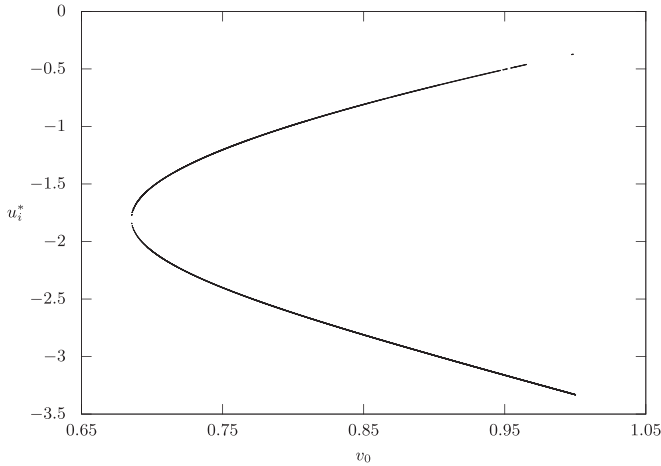


FIG. 6. Saddle-node bifurcation of the system [Eq. (49)] against the parameter v_0 . All variables are normalized as before.

a fractal construction, signifying chaos. In Fig. 6, we have presented the bifurcation of the equilibrium point u_i^* against the parameter v_0 , which shows the existence of a saddle-node bifurcation in the system.

IV. HYBRID-PIC-MCC SIMULATION OF DUSTY PLASMA

Our simulation model comprises a 1D electrostatic particle-in-cell (PIC) code with the capability of having various boundary conditions including periodic boundary [8–10]. We note that the usual PIC model does not have any collisional transfer of momenta. Also, the particles in a PIC model are macroparticles comprising a number of real-life particles. As such, any collision implemented under the PIC formalism will actually account for collisions *en masse*. However, in a limited way, collisions can be implemented in a PIC formalism through PIC-Monte Carlo collision (PIC-MCC) algorithm. It consists of using a randomized probability to account for the collisions based on the theoretical estimation of the collision cross sections. A multistep Monte Carlo collision is also another way of including collisions [32]. We rather use a hybrid method to estimate the collisions of dust particles with electrons and ions, which is described as the *hybrid*-PIC-MCC (*h*-PIC-MCC) method [9,10]. In this code, the computational dust particles are named *dust sites*, which are fixed in space. Altogether, we use about ~ 2500 – 3000 dust sites which account for an equivalent dust density of $\sim 10^{12} \text{ m}^{-3}$ (see the next section for details). We have used a plasma density of 10^{16} m^{-3} , which is simulated with 10^5 numbers of computational particles each for ions and electrons. The domain of simulation is $\sim 0.01 \text{ m}$. The details of this algorithm and the code are described in the two papers by Changmai and Bora [8,9].

A. Dust-charge fluctuation and plasma sheath

In order to account for the dust charge fluctuation in our simulation, we assume that whenever a collision of the dust particle with an electron occurs, it contributes to an increase of negative charge on the surface of the dust particle [9,10]. This is effected by decreasing the number of electrons in the simulation domain accompanied by an equivalent increase of

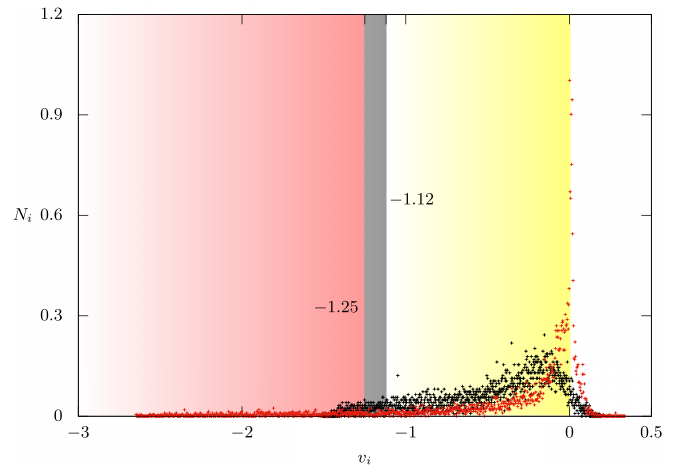


FIG. 7. Ion velocity distributions in the sheath region (up to about $x \lesssim 10\lambda_D$) with and without dust-charge fluctuation. While the black points indicate the distribution with constant dust charge, the red points indicate the same with dust-charge fluctuation. See the accompanying text for an explanation about the different regions indicated in the figure. The sheath is on the left ($x = 0$), and the “–” sign indicates left-moving ions going toward the sheath. The velocity is normalized with the ion-sound speed.

electron dust charge number z_d . The accumulation of positive charge on the surface of a dust particle is, however, modeled by assuming that whenever an ion-collision occurs, an electron is ejected from the dust particle which causes z_d to decrease (equivalently charging the dust particle positively) and an increase of a plasma electron in the simulation box. Hence, the total ion number in the simulation domain remains constant while the total electron number and dust charge fluctuate depending on the type of collisions. Without loss of any generality, this process can be extended up to any number of dust particles, thereby simulating an environment of a dusty plasma.

In our simulation, we, however, assume that the dust particles are cold and stationary, which is consistent with the characteristic timescale of the simulation, i.e., a dust-ion-acoustic timescale, and this is also what we consider in the theoretical buildup. We also introduce a randomized probability $p_{i,e}$, which determines whether a charged particle is absorbed by a dust particle in the event of a collision, hence the name *h*-PIC-MCC. At this point, it should be noted that every binary collision in this formalism is a collision between two macroparticles, which in reality does not happen. Nevertheless, in the dust-ion-acoustic timescale, this procedure is able to capture the essential physics involving dust-ion-acoustic (DIA) dynamics. For all practical purposes, the dust particles act as collections of electrons, assuming that the dust particles charge to a net negative potential as the plasma attains its equilibrium. Our prescription for dust charging conserves the plasma quasineutrality condition

$$n_i = n_e + z_d n_d. \quad (59)$$

The dust macroparticles are uniformly distributed in the domain with zero net charge. The dust radius is fixed at $r_d \sim 10^{-2} \lambda_{De}$. As mentioned before, in Fig. 1, the average charging of a single dust particle is shown, calculated from the total

count of electron depletion in the simulation domain. As can be seen from the figure, on average, a single dust particle attains an equilibrium net charge of about $Q_d \sim -1000e$. The equivalent dust number density can be calculated from the quasineutrality condition as $n_d \sim 2.1 \times 10^{12} \text{ m}^{-3}$.

$$M_c^2 = \frac{-\delta_i + 2q_{d0} + \sqrt{(3\delta_i - 2q_{d0})^2 + 8(\delta_i - 1)[2 - (3\delta_i - 2)/q_{d0}]}}{2[1 - (\delta_i - 1)/q_{d0}]}, \quad (60)$$

where q_{d0} is the normalized dust charge at the sheath edge. For the plasma parameters as mentioned in the previous paragraph, $M_c \simeq 1.12$ for constant dust charge and gets modified to $M_c \simeq 1.25$ in the presence of dust-charge fluctuation. In Fig. 7 we show the ion velocity distribution in the sheath region. Note that the sheath region extends *only* up to about $\sim 10\lambda_D$ (see the first panel in Fig. 2). In Fig. 7 we show the distributions for dust particles with constant charge (black dots) and with charge fluctuation (red dots). As expected, the penetrating velocity of the ions into the sheath increases in the presence of dust-charge fluctuation. Different regions indicated in the figure represent the presheath region, sheath edge for constant dust charge, and sheath edge with dust-charge fluctuation. The respective sheath edges are defined through the values $M = M_c$ and the presheath region is defined when the ion velocity is just zero demarcating the left- and right-moving ions. So, in this case, we define the presheath region as where ions have *just* started to move toward the left, i.e., toward the sheath. The number of ions in the figure is normalized by its maximum value.

B. Driven dust-charge fluctuation: Chaotic ion dynamics

We now consider the case for driven dust-charge fluctuation, where we drive the dust-charge fluctuation through a controlled emission of photoelectrons from the sheath-side wall by periodically exposing the wall to strong UV radiation. The periodic emission of photoelectrons can be mathematically represented (in the photoemission current to the dust particles) as

$$I_{hv} = \varrho \cos(\nu t)^{2\Delta}, \quad \Delta \gg 1 \text{ (integer)}, \quad (61)$$

where $2\pi/\nu$ is the periodicity of the photoemission burst (see Fig. 8) and ϱ is its amplitude. In our case, $\nu^{-1} \sim 0.04$, time being normalized by ω_{pi}^{-1} . Equation (61) is the same as Eq. (53), except that it is now in the photoemission current to the dust particles which has the same role in our simulation scenario as Eq. (53) in the theoretical formalism.

As we have periodic photoelectron bursts from the sheath-side wall, the plasma sheath oscillates between a classical sheath and an inverse sheath. This oscillation can be clearly seen from the reconstruction plots of the ion velocity distribution as shown in Fig. 9. The first panel of the plots shows the time evolution of the ion distribution function in the near-sheath region, while the second panel shows the evolution of the sheath as one moves away from the wall. We can clearly see the periodic formation of ion-velocity peaks in the first panel. In the second panel, we can see that the ion velocity distribution gradually approaches a Maxwell distribution as

We now present the results of our *h*-PIC-MCC simulation on the effect of dust-charge fluctuation. We note that the Bohm criterion for a plasma sheath with cold ion and constant dust charge is $M > M_c = \sqrt{\delta_i}$, which gets modified for dust-charge fluctuation [6]

one goes away from the wall. In Fig. 10 we show the chaotic evolution of the ion velocity distribution in the sheath and the near-sheath region. It should, however, be noted that in the presence of the driven photoemission, there is no clear sheath boundary as the sheath itself oscillates in time. We show the power spectral density \mathcal{P} of these oscillations (first panel, first row of Fig. 10) in the second panel of the third row of Fig. 10. The spectral density shows a dominant peak at the frequency ~ 0.354 corresponding to an angular frequency of $\omega \sim 2.22$, which is the large-scale oscillation that we see. The second dominant peak in \mathcal{P} away from the large-scale oscillations is at a frequency ~ 3.47 corresponding to an angular frequency of $\omega \sim 21.79$ which represents the fine-scale oscillations. These fine-scale oscillations actually correspond to the frequency of the driven photoemission bursts frequency shown in Fig. 8, represented by Eq. (61). So what we see is that the periodic bursts of photoemission of electrons are exciting very low-frequency large-scale oscillations in ion velocity through dust-charge fluctuations.

We initially perform two different tests for chaos on the ion velocity distributions: (1) estimation of the dominant Lyapunov exponent l from a time series with the help of Wolf's algorithm [33] and (2) performing 0-1 test for chaos. While Wolf's method calculates the dominant Lyapunov exponent through reconstruction of the phase space (also referred to as *delay reconstruction*) from the time series data and detection of orbital divergence, the 0-1 test estimates the growth rate

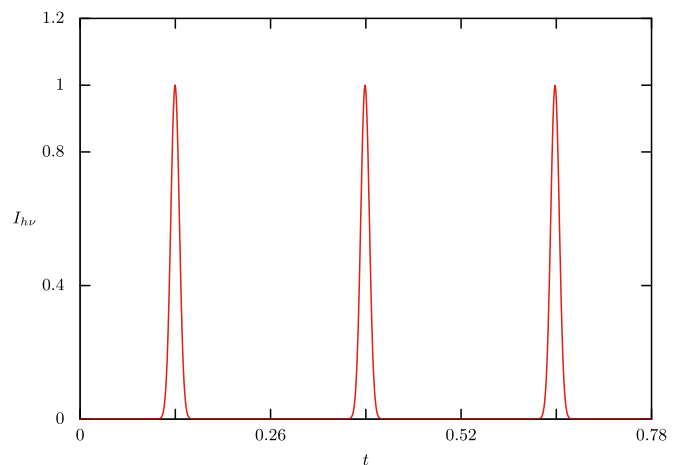


FIG. 8. Periodic burst of photoemission. The time is measured in the units of the ion-plasma period. The current is normalized by its peak value.

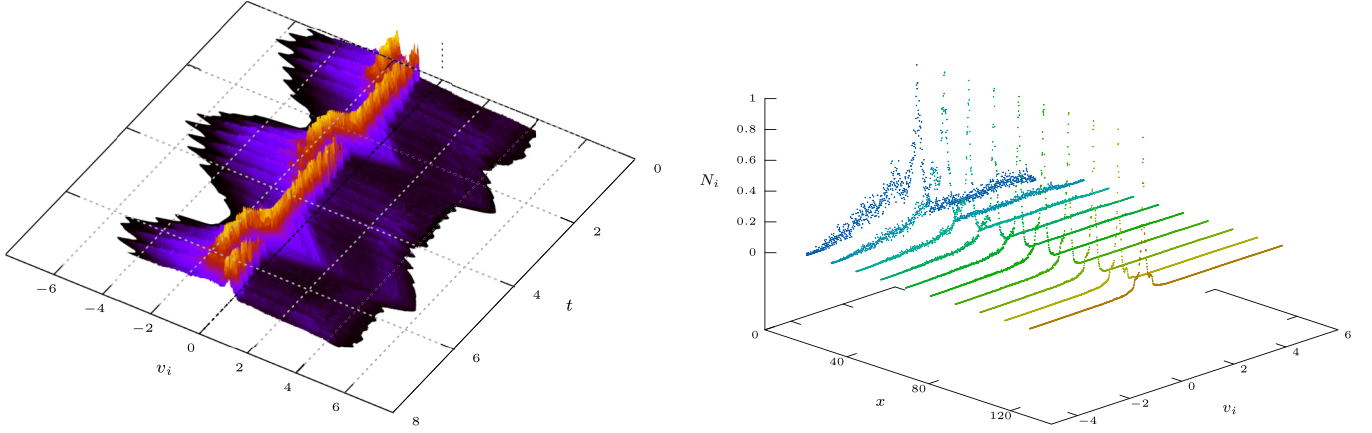


FIG. 9. Evolution of the plasma sheath in time (first panel) and in space (second panel) in terms of ion velocity distribution. In the first panel, the ion velocity distribution is plotted in the near-sheath region in time, where the oscillation of the sheath (in terms of periodic peaking of ion velocity) can be clearly seen. In the second panel, the ion velocity distribution function is plotted as one moves away from the sheath (the wall is at $x = 0$). As before, x is measured in the units of electron Debye length λ_{De} and velocity is normalized by the ion-sound speed.

of divergence from the time-averaged mean square displacement of the time series data. We use Wolf's algorithm as provided by the authors through their very well-developed Matlab/Octave interface. In the case of the 0-1 test, we use a very recent work involving the Chaos Decision Tree Algorithm by Toker *et al.* [34] to rule out stochasticity and random noise. Briefly, in the 0-1 test, two 2D systems $p(n)$ and $q(n)$ are derived from the 1D time series data $v(n)$ for $n = 1, 2, \dots$:

$$p(n+1) = p(n) + v(n) \cos(cn), \quad (62)$$

$$q(n+1) = q(n) + v(n) \sin(cn), \quad (63)$$

where $c \in [0, 2\pi]$ is random. For a particular c , the solution to Eqs. (62) and (63) requires

$$p_c(n) = \sum_{j=1}^n v(j) \cos(jc), \quad (64)$$

$$q_c(n) = \sum_{j=1}^n v(j) \sin(jc). \quad (65)$$

It can be shown that if $v(n)$ are regular, p, q are bounded, while they display asymptotic Brownian motion if $v(n)$ are chaotic. The time-averaged mean squared displacement of p, q is then calculated as

$$\begin{aligned} \mathcal{M}_c(n) = & \frac{1}{N} \sum_{j=1}^N \{ [p_c(j+n) - p_c(j)]^2 \\ & + [q_c(j+n) - q_c(j)]^2 \} + \sigma \eta_n, \end{aligned} \quad (66)$$

where $\eta_n \in [-1/2, +1/2]$ is a uniform random deviate and σ is the noise level for a total of N number of sampled data in the time series. Finally, the growth rate K is calculated as

$$K = \lim_{n \rightarrow \infty} \frac{\log \mathcal{M}_c(n)}{\log n}. \quad (67)$$

For chaotic data the median $K \rightarrow 1$ and for periodic system $K \rightarrow 0$.

In Fig. 11 we show the determined values of l and K from these two tests, and as can be seen, both tests point to the fact that the sampled data are indeed chaotic in nature.

1. Recurrence plots

As a final test, we construct the recurrence plots [35,36] for the oscillations shown in Fig. 10. The purpose of a recurrence plot is to visualize the recurrences of a dynamical system. It is a very powerful tool that enables us to construct complex dynamical patterns from a single time series. In summary, a recurrence plot is based on the following recurrence relation [36]:

$$\mathbf{R}_{ij} = \begin{cases} 1: & \bar{x}_i \approx \bar{x}_j, \\ 0: & \bar{x}_i \not\approx \bar{x}_j \end{cases} \quad i, j = 1, 2, \dots, N, \quad (68)$$

where the $\{\bar{x}_i\}_{i=1}^N$ is a system in its phase space and N is the number of considered states. Essentially $\mathbf{R}_{i,j}$ is a Heaviside function which depends on a threshold condition ε which determines whether $\bar{x}_i \approx \bar{x}_j$. If we assume that the state of a dynamical system $\bar{x}(t)$ is specified by d components, we can a form vector with these components [36]

$$\bar{x}(t) = (x_i(t))^T, \quad i = 1, 2, \dots, d \quad (69)$$

in the d -dimensional phase space. In a purely mathematically constructible setup, all these components are known and one can easily construct the phase space. However, in experiments and in a simulation like ours, we have only *one* time series with only one observable, which in this case is the ion velocity. So we have one discrete time series

$$u_i, \quad i = 1, 2, \dots, N, \quad (70)$$

with Δt as the sampling interval on the basis of which we have to reconstruct the phase space with the help of a time delay, as mentioned before [36],

$$\bar{x}_i = \sum_{j=1}^m u_{i+(j-1)\tau} \bar{e}_j, \quad \bar{e}_i \cdot \bar{e}_j = \delta_{ij}, \quad (71)$$

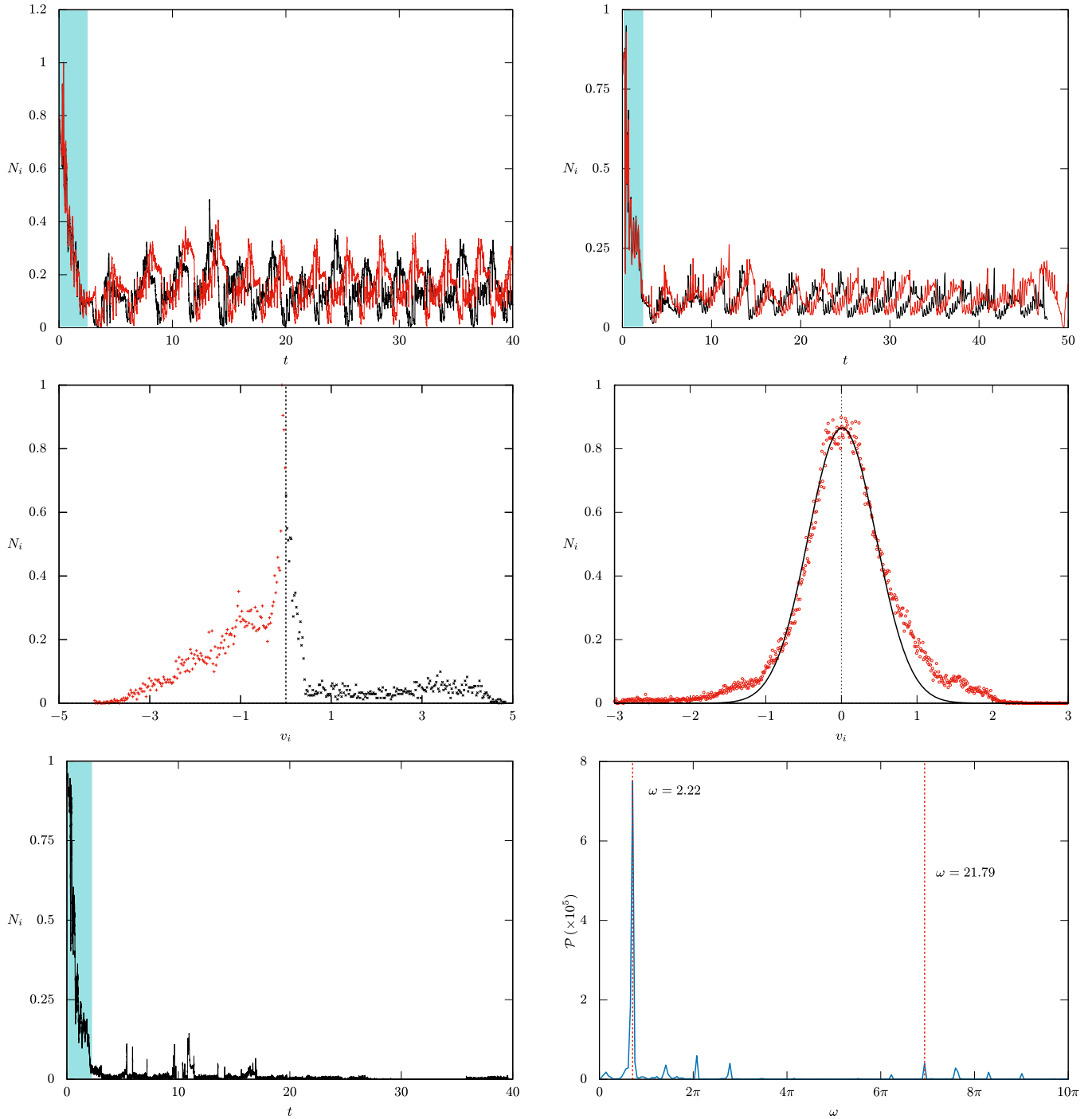


FIG. 10. First row: Two snapshots of the ion velocity distribution in the sheath and the near-sheath region for two different dust densities. The first panel is for $n_d \sim 2.1 \times 10^{12} \text{ m}^{-3}$, and the second one is for $n_d \sim 1.5 \times 10^{12} \text{ m}^{-3}$. Both plots show the characteristics signature of chaotic dynamics as confirmed by our chaos analysis. The shaded regions in both plots indicate initial transient regions as the distributions evolve in time. The change in oscillation patterns in both plots corresponds to a change of $\sim 10^{-4}$ in the burst duration of the emission of photoelectrons, and the periodicity of the bursts is same in all the cases. Second row: The ion distribution function in the sheath region and in the bulk plasma. Third row: The ion distribution function in the presence of periodic photoemission bursts as in the first cases but without any dust-charge fluctuation. The distribution is purely stochastic (left). The right panel shows the power spectral density \mathcal{P} of these oscillations shown in the left panel of the first row of this figure. All the parameters are in normalized units. See the text for details.

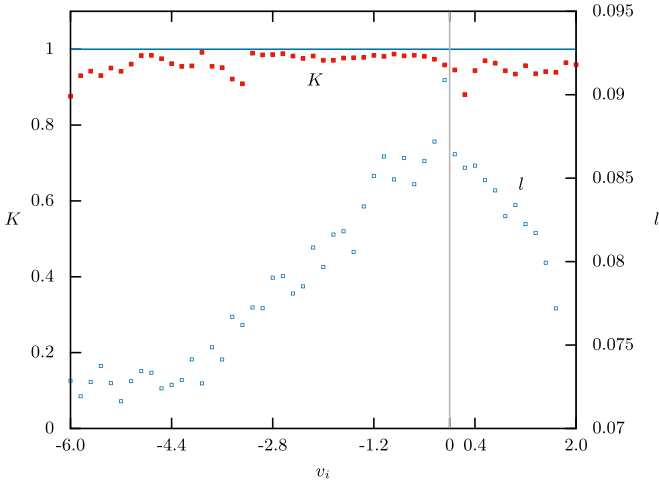


FIG. 11. Estimate of the dominant Lyapunov exponent as determined through Wolf's algorithm (right axis) and the K values from the 0-1 test (left axis) for the two sampled data shown in the first row of Fig. 10. The velocity is normalized by the ion-sound speed.

where m is the embedding dimension, τ is the time delay, and \vec{e}_j are the unit vectors that span an orthogonal system. For $m \geq 2D_2 + 1$, where D_2 is the correlation dimension of the underlying attractor, with the help of Taken's theorem one can show the existence of a *diffeomorphism* between the original and the reconstructed phase space, or simply speaking, one can use the reconstructed attractor to study the original one but in a different coordinate system. So our recurrence plot is then defined by the relation

$$\mathbf{R}_{ij}(\varepsilon) = H(\varepsilon - \|\vec{x}_i - \vec{x}_j\|), \quad i, j = 1, 2, \dots, N, \quad (72)$$

where N is the number of measured points, $H(x)$ is the Heaviside step function, and $\|\cdot\|$ denotes norm. In our case we have used an Euclidean L_2 norm.

In Fig. 12 we have shown six recurrence plots for the chaotic oscillations shown in Fig. 10. The embedding dimension is chosen to be 4 and the delay used is 5. The threshold is used about $\sim 8.9\%$ of the maximum amplitude of the oscillations. Clockwise from the top in the figure, we have used a sampling interval $t_{\text{sample}} = 2, 10, 50, 100$, respectively, over a total of 32 500 time steps Δt . We can see that as the sampling interval increases, the plots increasingly reveal the signature of a chaotic oscillation, signifying the small fine-scale periodic oscillations in the first plot with geometric recurrences when the sampling interval is small (the first plot in the first row) and a fractal pattern in the last of these four plots (the second plot in the second row). The first plot in the third row is similar to the second plot of the second row except that we have superimposed the corresponding plot with a map having no threshold (all recurrences). The last plot in the figure represents the one for ion velocity distribution time series with constant dust charge, corresponding to the last plot of Fig. 10. As one can see that this plot is similar to the one with random dynamics similar to Brownian motion signifying stochastic behavior [36].

V. CONCLUSION

To summarize, in this work in brief, we consider a plasma model where electrons and ions are both thermal particles having cold and stationary dust grains with constant dust density. The time scale of our interest is the dust-ion-acoustic time scale. We develop the sheath equations and solve them numerically with a hybrid approach coupling the initial value problem of the dust-charging equation with the boundary value problem of the nonlinear Poisson's equation. The whole theoretical formalism has been also replicated using a *hybrid-PIC-MCC* simulation, and the theoretical results are found to be in good agreement with the simulation results.

Next, we consider the case for *driven* dust-charge fluctuation, which is the primary focus of this work. We use the plasma sheath as a candidate to induce periodic dust-charge fluctuation through photoemission. The photoemission occurs when the sheath-side wall is exposed to UV radiation. So, by externally exposing the wall to UV radiation, the dust-charge fluctuation can be driven at an external frequency. Here, in the dust-ion-acoustic regime, we focus on the ion dynamics in the sheath and the presheath regions. We show that the relatively high-frequency, of the order of about $\sim 3.5\omega_{pi}$, bursts of photoemission of electrons from the plasma sheath excite a chaotic superharmonic large low-frequency wave in ion velocity through dust-charge fluctuation, which is confined to the sheath and the presheath regions. With the help of appropriate analysis, we have established that the oscillations are indeed chaotic which owes its existence to the harmonic variation of the dust-charge fluctuation. The oscillations remain stochastic for constant dust-charge showing that in the absence of dust-charge fluctuation, the sheath oscillations cannot effectively propagate to the plasma.

As the topic of this work is exploratory in nature, we provide a future prospect for the work in brief. Going by the number of hydrodynamic equations of this electrostatic model, Eqs. (44)–(46), along with Eq. (53) for externally driven dust-charge fluctuation, it can be termed as a *four-field* fluid model. Naturally, any extra physics in terms of dust particle dynamics or introduction of an external magnetic field will increase the *dimensionality* of the system and which in turn will provide more exploratory ground for nonlinear phenomena. In particular, as any wave associated with dust dynamics will be necessarily extremely low frequency (compared to the ion-acoustic frequency), we expect some interesting dynamics in the dust-acoustic domain. Any interaction among dust particles might also lead to interesting physics as in the dust-acoustic regime, there are many reports about the formation of dust-crystal or lattice-like structures [37–39]. How an external driving force interacts with these structures remains to be seen in the near future and might lead to the design of new and innovative experiments. In this context, self-organization and transition of strongly coupled dusty plasma, forming a 2D dusty plasma under periodic substrate, is also noteworthy [40–43].

There are also many studies involving oblique magnetic field and plasma sheath [44–46]. However, how an external driving mechanism changes the sheath structure is a topic about which we still do not have much knowledge. As a magnetic field essentially restricts particle movement in the

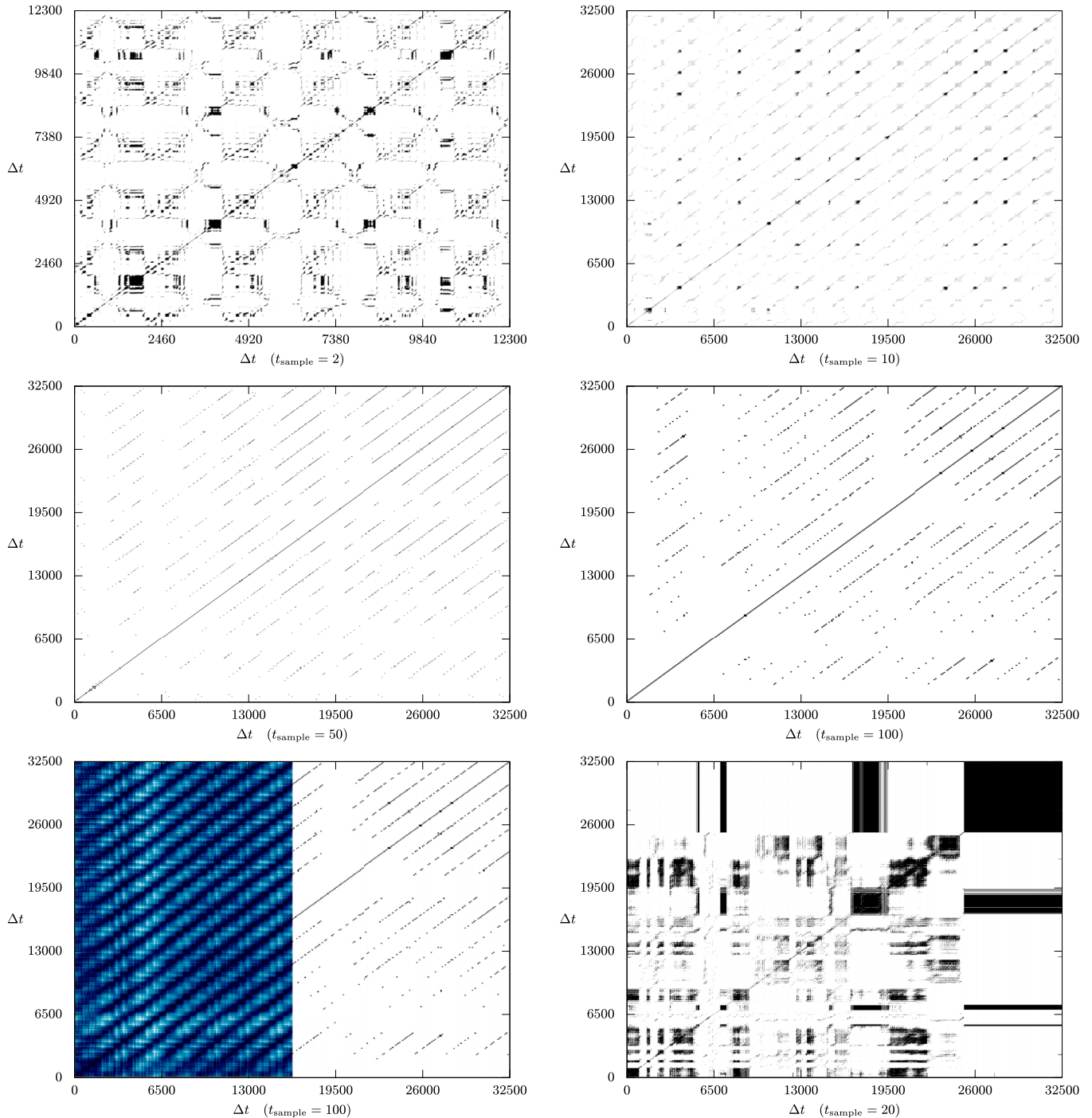


FIG. 12. First and second rows: Recurrence plots for the chaotic oscillation shown in Fig. 10 for different sampling intervals. Third row: Same as the second plot of the second row, superimposed with a map with no threshold, displaying all recurrences (left) and a plot for a nonchaotic oscillation with constant dust-charge, displaying the signature for Brownian motion-like pattern.

perpendicular direction, we might observe suppression of these chaotic oscillations with an oblique (with respect to the sheath) magnetic field, but the subject, however, is beyond the purview of the present work.

Another related phenomenon is the avalanche excitations of fast particles in a quasi-2D cold dusty plasma liquid. In these systems, noise can even induce spatiotemporal coherence [47–49]. It will be interesting to see signatures of

chaos in these systems, though they are vastly different from what we consider in this work.

ACKNOWLEDGMENTS

The authors thank the anonymous referees for their constructive and critical suggestions.

APPENDIX: CALCULATION OF ARBITRARY γ

Equations (44) and (45) for arbitrary γ are given by

$$\frac{\partial n_i}{\partial \tau} - \frac{1}{v_0} \frac{\partial}{\partial \tau} (n_i u_i) = 0, \quad (\text{A1})$$

$$\frac{\partial u_i}{\partial \tau} - \frac{u_i}{v_0} \frac{\partial u_i}{\partial \tau} - \gamma \sigma n_i^{\gamma-2} \frac{1}{v_0} \frac{\partial n_i}{\partial \tau} = \frac{1}{v_0} \frac{\partial \phi}{\partial \tau}. \quad (\text{A2})$$

Integration of Eq. (44) [or Eq. (A1)] and using the boundary conditions $u_i(\tau) \rightarrow u_0$ and $n_i(\tau) \rightarrow n_{i0} \equiv 1$ at infinity, we have, as before

$$n_i = \frac{v_0 - u_0}{v_0 - u_i}. \quad (\text{A3})$$

Equation (A2) can be integrated to have

$$\phi = \frac{1}{2} (u_0^2 - u_i^2) - v_0 (u_0 - u_i) - \frac{\gamma \sigma}{(\gamma - 1)} \left[1 - \left(\frac{u_0}{u_i} \right)^{\gamma-1} \right], \quad (\text{A4})$$

where we have used the condition that

$$M = n_i u_i \equiv u_0. \quad (\text{A5})$$

Equation (A4) reduces to Eq. (48) for $\gamma = 2$.

Let's now find out by how much ϕ differs, if we deviate from $\gamma = 5/3$, the standard value for a monoatomic gas. Let us denote the difference between γ and the standard value $5/3$

as δ ,

$$\delta = \gamma - \frac{5}{3}. \quad (\text{A6})$$

Inserting γ in terms of δ in Eq. (A4) and expanding around $\delta \rightarrow 0$, we obtain the correction term in ϕ to the order $O(\delta)$ as

$$\phi_{\text{correction}} = \left| \delta \sigma \left\{ \frac{5}{2} \left(\frac{u_0}{u_i} \right)^{2/3} \ln \left(\frac{u_0}{u_i} \right) + \frac{9}{4} \left[1 - \left(\frac{u_0}{u_i} \right)^{2/3} \right] \right\} \right|. \quad (\text{A7})$$

Let us now assume that the ion velocity u_i differs from its value at infinity u_0 by an amount $\Delta u = u_i - u_0$ at any point of time. If we now consider the limiting values of $\phi_{\text{correction}}$ when either $\Delta u \rightarrow 0$ or $\Delta u \rightarrow \infty$ ($\gg 1$), we have

$$\lim_{\Delta u \rightarrow 0} \phi_{\text{correction}} = 0, \quad (\text{A8})$$

$$\lim_{\Delta u \rightarrow \pm\infty} \phi_{\text{correction}} = \frac{9}{4} \delta \sigma. \quad (\text{A9})$$

The value of the latter for $\delta = 1/3$ (if we take $\gamma = 2$ instead of $5/3$) and $\sigma = 0.01$ (the typical value of sigma used in these calculations) is ~ 0.0075 , which is $\ll |\phi_{\text{wall}}|$, considering the fact that at the wall only ϕ can attain its maximum value. Note that Δu is also expected to be maximum only at the wall.

The above calculation shows that even if we replace $\gamma = 2$ for these calculations, this is not expected to make a huge difference in the results obtained.

-
- [1] S. Basnet, R. R. Pokhrel, and R. Khanal, *IEEE Trans. Plasma Sci.* **49**, 1268 (2021).
- [2] G. C. Das, R. Deka, and M. P. Bora, *Phys. Plasmas* **23**, 042308 (2016).
- [3] H. Mehdipour, I. Denysenko, and K. Ostrikov, *Phys. Plasmas* **17**, 123708 (2010).
- [4] B. P. Pandey and A. Dutta, *Pramana J. Phys.* **65**, 117 (2005).
- [5] M. R. Jana, A. Sen, and P. K. Kaw, *Phys. Rev. E* **48**, 3930 (1993).
- [6] P. K. Shukla and A. A. Mamun, *Introduction to Dusty Plasma Physics* (Institute of Physics, Bristol, 2002).
- [7] P. K. Shukla and V. P. Silin, *Phys. Scr.* **45**, 508 (1992).
- [8] S. Changmai and M. P. Bora, *Phys. Plasmas* **26**, 042113 (2019).
- [9] S. Changmai and M. P. Bora, *Sci. Rep.* **10**, 20980 (2020).
- [10] S. Changmai, Ph.D. thesis, Gauhati University, Guwahati, India, 2022.
- [11] A. Piel, F. Greiner, T. Klinger, N. Krahnstöver, and T. Mausbach, *Phys. Scr. T* **84**, 128 (2000).
- [12] M. Megalingam, A. Sangem, and B. Sarma, *Contrib. Plasma Phys.* **60**, e201900189 (2020).
- [13] B. Buti, *Pramana J. Phys.* **49**, 93 (1997).
- [14] C. S. Kueny and P. J. Morrison, *Phys. Plasmas* **2**, 1926 (1995).
- [15] D.-G. Dimitriu and M. Agop, in *Handbook of Applications of Chaos Theory*, edited by C. H. Skiadas and C. Skiadas (CRC Press, New York, 2016), pp. 321–424.
- [16] J. Levy, M. S. Sherwin, and J. Theiler, *Phys. Rev. Lett.* **70**, 2597 (1993).
- [17] J. Levy, M. S. Sherwin, and J. Theiler, *Phys. Rev. B* **48**, 7857 (1993).
- [18] R. K. Varma, P. K. Shukla, and V. Krishan, *Phys. Rev. E* **47**, 3612 (1993).
- [19] M. Momeni, I. Kourakis, M. Moslehi-Fard, and P. K. Shukla, *J. Phys. A: Math. Theor.* **40**, F473 (2007).
- [20] A. Sen, S. Tiwari, S. Mishra, and P. Kaw, *Adv. Space Res.* **56**, 429 (2015).
- [21] F. Cichocki, M. Merino, and E. Ahedo, *Acta Astronaut.* **146**, 216 (2018).
- [22] S. H. Strogatz, *Nonlinear Dynamics and Chaos: With Applications to Physics, Biology, Chemistry, and Engineering* (CRC Press, 2018).
- [23] S. E. Newhouse, D. Ruelle, and F. Takens, *Commun. Math. Phys.* **64**, 35 (1978).
- [24] F. Jinqing and Z. Liulai, *Nucl. Instrum. Methods Phys. Res., Sec. B* **26**, 259 (1987).
- [25] D. F. Escande, *Plasma Phys. Control. Fusion* **58**, 113001 (2016).
- [26] M. V. Nezlin, *Plasma Phys.* **10**, 337 (1968).
- [27] R. Deka and M. P. Bora, *Phys. Plasmas* **27**, 043701 (2020).
- [28] R. Deka and M. P. Bora, *Phys. Plasmas* **25**, 103704 (2018).
- [29] R. Z. Sagdeev, in *Reviews of Plasma Physics*, edited by M. A. Leontovich, Vol. 4 (Consultants Bureau, New York, 1966), p. 23.
- [30] M. P. Bora and D. Sarmah, [arXiv:0708.0684v1](https://arxiv.org/abs/0708.0684v1).
- [31] A. C.-L. Chian, F. A. Borotto, T. Hada, R. A. Miranda, P. R. Muñoz, and E. L. Rempel, *Rev. Mod. Plasma Phys.* **6**, 34 (2022).
- [32] N. A. Gatonis, R. E. Erlandson, and C.-I. Meng, *J. Geophys. Res.* **99**, 8479 (1994).

- [33] A. Wolf, J. B. Swift, H. L. Swinney, and J. A. Vastano, *Phys. D: Nonlinear Phenom.* **16**, 285 (1985).
- [34] D. Toker, F. T. Sommer, and M. D'Esposito, *Commun. Biol.* **3**, 11 (2020).
- [35] J.-P. Eckmann, S. O. Kamphorst, and D. Ruelle, *Europhys. Lett.* **4**, 973 (1987).
- [36] N. Marwan, M. C. Romano, M. Thiel, and J. Kurths, *Phys. Rep.* **438**, 237 (2007).
- [37] V. E. Fortov *et al.*, *J. Phys. A: Math. Gen.* **39**, 4533 (2006).
- [38] J. Maddox, *Nature (London)* **370**, 411 (1994).
- [39] C. M. Ticos, C. P. Lungu, P. Chiru, I. Mustata, and V. Zaroschi, Dust crystal interaction with plasma flows, in *2009 IEEE International Conference on Plasma Sciences, San Diego* (IEEE, New York, 2009), p. 1.
- [40] Y. Huang, C. Reichhardt, C. J. O. Reichhardt, and Y. Feng, *Phys. Rev. E* **106**, 035204 (2022).
- [41] W. Zhu, C. Reichhardt, C. J. O. Reichhardt, and Y. Feng, *Phys. Rev. E* **106**, 015202 (2022).
- [42] L. Gu, W. Li, C. Reichhardt, C. J. O. Reichhardt, M. S. Murillo, and Y. Feng, *Phys. Rev. E* **102**, 063203 (2020).
- [43] W. Li, K. Wang, C. Reichhardt, C. J. O. Reichhardt, M. S. Murillo, and Y. Feng, *Phys. Rev. E* **100**, 033207 (2019).
- [44] Z. Xiu, *Chinese Phys. Lett.* **23**, 396 (2006).
- [45] T.-T. Wang, J. X. Ma, and Z.-A. Wei, *Phys. Plasmas* **22**, 093505 (2015).
- [46] J.-Y. Liu *et al.*, *Vacuum* **80**, 1206 (2006).
- [47] Y.-J. Lai and Lin I, *Phys. Rev. Lett.* **89**, 155002 (2002).
- [48] H.-W. Hu, Y.-C. Zhao, and L. I, *Phys. Rev. Res.* **4**, 023116 (2022).
- [49] L.-W. Teng, P.-S. Tu, and L. I, *Phys. Rev. Lett.* **90**, 245004 (2003).